
Contrast-Enhanced MRI and Micro-CT Adopted for Evaluation of a Lipid-Lowering and Anticoagulant Herbal Epimedium-Derived Phytoestrogenic Extract for Prevention of Steroid-Associated Osteonecrosis

Ling Qin (✉)¹, Ge Zhang¹, Hui Sheng¹, James F. Griffith², Ka Wai Yeung²,
and Kwok-Sui Leung¹

¹ Department of Orthopaedics and Traumatology, The Chinese University of Hong Kong,
Hong Kong, China
e-mail: lingqin@cuhk.edu.hk

² Department of Radiology and Organ Imaging, The Chinese University of Hong Kong,
Hong Kong, China

Abstract

We developed an alternative steroid-associated osteonecrosis (ON) rabbit model using a combination of a single injection of low-dose lipopolysaccharide (LPS) and three subsequent injections of pulsed high-dose methylprednisolone (MPS). The usefulness of this experimental ON model was evaluated using both conventional and advanced bio-imaging techniques, including contrast-enhanced dynamic MRI and a high-resolution micro-CT. Details on establishment of methodology are described, which were adopted into an efficacy study on a herbal Epimedium-derived phytoestrogenic extract (HEPE) developed for prevention of steroid-associated ON using an established rabbit model. The underlying mechanisms of HEPE for prevention of steroid-associated ON were found to be associated with inhibition of both intravascular thrombosis and extravascular bone marrow lipid deposition, the two known mechanistic pathways in pathogenesis of ON. Our experimental results provide for potential clinical trials or applications of HEPE in the prevention of ON among high-risk patients undergoing steroid treatment.

Introduction

Indications of Steroids and Its Side Effects Related to Osteonecrosis

Osteonecrosis (ON) is a severe skeletal disease that can result from trauma, alcohol abuse, and life-saving pulsed steroid. Steroids are routinely indicated for treatment of many medical conditions such as rheumatoid arthritis (RA), infectious diseases,

organ transplantation, and hemodialysis (Assouline-Dayana et al. 2002). Epidemiologic survey shows that there are approximately 20,000 new ON patients diagnosed per year in U.S., and the prevalence of ON in Asia is even two to three times higher (National Osteonecrosis Foundation; Wang et al. 2004). Steroid-associated ON has even become a socio-economic problem in Hong Kong and mainland China since the outbreak of several virus infectious diseases, including severe acute respiratory syndrome (SARS; Griffith et al. 2005; Li et al. 2006; Hong and Du 2004; Koller et al. 2000; Miller et al. 2002; Scribner et al. 2000; Shen et al. 2004; So et al. 2003).

The pathogenesis of steroid-induced ON is thought to be intravascular thrombosis-induced occlusion and extravascular lipid-deposit-induced compression, leading to an impaired structure-function of intraosseous blood supply system. The impaired intraosseous blood supply induces ischemia, necrosis lesion, and subchondral bone collapse. Some patients may end up with total joint replacement (Aaron et al. 1998; Assouline et al. 2002; Lieberman et al. 2002; Qin et al. 2006; Wang et al. 2000). Unfortunately, the prognosis of total joint replacement is not satisfactory, especially in patients with steroid-induced ON (Aaron et al. 1998; Saito et al. 1989). This implies that prevention of ON development is essential for high-risk patients, including those undergoing steroid treatment (Qin et al. 2006; Wang et al. 2000).

Research and Development in Prevention of Steroid-Associated ON

Based on the pathogenesis of steroid-associated ON, anti-thrombosis agents, such as warfarin, and lipid-lowering agents, such as statins, have been clinically used to prevent steroid-associated ON; however, due to side effects (bleeding for warfarin and abnormalities in liver for statins) occurring during long-term administration, their routine clinical use for prevention of steroid-associated ON among risk patients is limited (Expert Panel 2001; Glueck et al. 2005; Martin et al. 2004; Motomura et al. 2004; Pritchett et al. 2001; Wortmann et al. 2002; Schulman et al. 1999; Wang et al. 2000). It is therefore highly desirable to develop therapeutic agents for long-term use that may target both intravascular thrombosis and extravascular lipid deposition, with fewer no side effects for preventing steroid-induced ON.

The SARS outbreak in China in 2003 provided a unique opportunity where a remarkable difference in incidence of steroid-associated ON was diagnosed using MRI, with up to 32.7% ON (23% ON at hip alone) found in SARS patients in Beijing (Li et al. 2005), whereas only 5–6% in Hong Kong and Guang Zhou (Griffith et al. 2005; Shen et al. 2004). Apart from potential dose variations in steroid use, frequency of herb preparation used for SARS patients during pulsed steroid treatment was much higher in southern China (Hong Kong and Guang Zhou) than in North China (Beijing); thus, we speculate that the much lower ON incidence in Hong Kong and Guang Zhou might be attributed to potential preventive effects of herbs involved in conventional anti-inflammatory traditional herbal medicine including phytoestrogenic extraction from herbal *Epimedium* during life-saving standard pulsed steroid for treatment of SARS patients (Lau and Leung 2005; Liu et al. 2006), whereas no such conventional approach was introduced for treatment of SARS patients in Beijing (Li et al. 2005).

Herbal *Epimedium* is known as a kidney-tonifying “bone-strengthening” herb. An *Epimedium*-derived phytoestrogenic extract (HEPE) has been developed as an alternative preparation for long-term and safe administration to prevent postmenopausal osteoporosis (Qin et al. 2005a,b; Zhang et al. 2006). To date, a group of phytoestrogen fractions have been derived from *Epimedium* by a series of standardized extraction and isolation procedures, which mainly consist of three phytoestrogenic compounds (Icariin, Genistein and Daidzein; Lee et al. 2004; Meng et al. 2005; Qin et al. 2005a).

Interestingly, phytoestrogen has also been shown to be able to decrease low-density lipoprotein and increase high-density lipoprotein (Anderson et al. 1995; Clifton-Bligh et al. 2001; Lamon-Fava et al. 2000). This may imply potential beneficial effects on reversing cholesterol transport, i.e., a potential capability in inhibiting lipid deposition in peripheral tissues. In fact, studies have shown that phytoestrogen also has potential anti-thrombotic activity through maintaining a balance between coagulation and fibrinolysis (Choo et al. 2002; Wang et al. 2004). These observations motivated the investigators of this chapter to establish the following hypothesis that HEPE might prevent steroid-associated ON through a unique mechanism associated with inhibition of both thrombosis and lipid deposition. In order to confirm this hypothesis, animal experiments are essential to investigate whether HEPE is able to prevent steroid-associated ON development experimentally, as no clinical trials with controlled conditions are ethically possible to confirm the above-mentioned epidemiologic observations.

Current Available Osteonecrosis Animal Models and Their Limitations

The steroid-associated ON animal models developed in the past include both quadrupeds (mice, rats, rabbits, dogs, pigs, dogs, and horses, etc.) and bipeds (chicken and emeses). All these models may not be able to produce joint collapse, which has been found in ON patients; however, they are still useful for studying the pathogenesis of steroid-associated ON and evaluation of pharmaceutical agents or biophysical means developed for prevention of ON development. Among the above-mentioned animal models, the rabbit ON model is the most frequently used model (Expert Panel 2001; Glueck et al. 2005; Lang et al. 1989; Martin et al. 2004; Motomura et al. 2004; Pritchett et al. 2001; Schulman et al. 1999; Qin et al. 2006; Wortmann et al. 2002; Wang et al. 2000).

Steroid-Associated ON in Rabbit Model

There are two protocols commonly used for establishing steroid-associated ON model in rabbits. One protocol is to use a single injection of high-dose methylprednisolone (MPS; i.e., H-MPS \times 1); however, this has a low incidence of ON (43%; Yamamoto et al. 1997). The other protocol is to use two injections of high-dose lippolysaccharide (LPS) combined with subsequent three injections of high dose MPS (i.e., H-LPS \times 2 – H-MPS \times 3), but this carries a high mortality (50%; Yamamoto et al. 1995). For developing intervention strategies for steroid-associated ON, there is a need to

develop protocols for establishing animal model with a high incidence but low mortality. Recently, a steroid-independent ON rabbit model was successfully established with a single injection of low-dose LPS, which showed a higher incidence of ON lesion (77%) and lower mortality (11%) as compared with the protocol (i.e., H-LPS \times 2–H-MPS \times 3) due to avoidance of severe LPS-induced shock by lowering the given dose (Irisa et al. 2001). The authors of this chapter recently confirmed that a single low-dose LPS injection combined with three subsequent injections of pulsed high-dose MPS did induce a high incidence of ON but low or even no mortality in rabbits (Qin et al. 2006). The first part of the chapter reviews the development of imaging methods for studying alterations of blood circulation under the influence of steroid treatment.

Development of a Steroid-Associated ON Rabbit Model

Animals and Inductive Protocols

Twenty-eight-week-old male New Zealand white rabbits with body weight of 45 kg were used. Fourteen rabbits were assigned to the treatment group and received LPS injection (i.v. 10 μ g/kg) (*Escherichia coli* 0111:B4, Sigma-Aldrich). Twenty-four hours later, three MPS injections (i.m. 20 mg/kg; Pharmacia and Upjohn) were given intramuscularly at a time interval of 24 h. Six rabbits were used as control and injected with 0.9% normal saline. The rabbits in both groups were killed 6 weeks after the last MPS injection (Qin et al. 2006).

Imaging Methods Established for Monitoring and Confirmation of ON Development

Contrast-Enhanced MRI for Monitoring Blood Perfusion In Vivo

Contrast-enhanced dynamic MRI was performed for bilateral proximal and distal femora before LPS injection and 6 weeks after the last injection of MPS, using a 1.5-T superconducting system (ACS-NT Intera; Philips, The Netherlands). An extremity coil (transmit-receive surface coil) was used on the target site of the rabbits under sedation with Katamin (i.m. 0.25 ml/kg). T1-weighted MRI images [repetition time (TR) / echo time (TE)=425/13 ms] were used for analysis of the target site with a section thickness of 3 mm. A total of 200 dynamic images were obtained in 90 s. A bolus of dimeglumine gadopentetate (0.8 mmol/kg; Magnevist, Schering, Berlin, Germany) was rapidly administered manually via a previously placed 21-gauge intravenous catheter in the right ear vein, immediately followed by a 6-ml saline flush at the same injection rate. The dynamic scan started as soon as the injection of the contrast medium commenced. Signal intensity (SI) was then measured in operator-defined ellipse-like regions of interest (ROIs) over the target site beneath the joint space in the mid-coronal T1-weighted images (Fig. 1) using a cursor and graphic display device. The SI values derived from the ROIs were plotted against time as time-intensity curve (TIC). The baseline value (SI_{base}) of the SI in a TIC was calculated as the mean SI value in the first three images. The maximum SI (SI_{max}) was defined as the peak enhancement value at a given time interval of 90 s after contrast injection

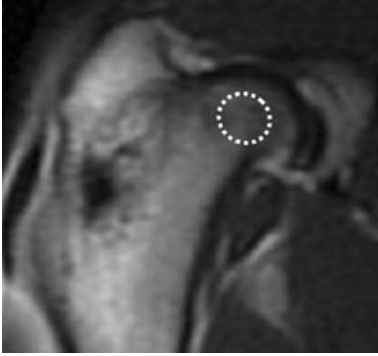


Figure 1. A T1-weighted coronal MRI image of rabbit proximal femur (TR/TE = 425/13 ms) after Gd-DTPA administration. The region of interest in the central part of femoral head with a size of 8 ~ 10 pixels (64 ~ 80 mm²) was defined for analysis of local intraosseous perfusion

during the early phase of the first pass. Perfusion index “maximum enhancement” was calculated as:

$$\text{Maximum enhancement} = \frac{\text{SI}_{\text{max}} - \text{SI}_{\text{base}}}{\text{SI}_{\text{base}}} \times 100\%$$

The mean of the maximum enhancement values measured at bilateral proximal femur of each rabbit was used for data analysis (Lang et al. 1989; Qin et al. 2006).

Development of a Micro-CT-Based Microangiography for Intraosseous Vessels

Under general anesthesia with sodium pentobarbital the abdomen cavity of the animals was opened and a scurf-needle with 25-mm syringe was inserted in the ab-

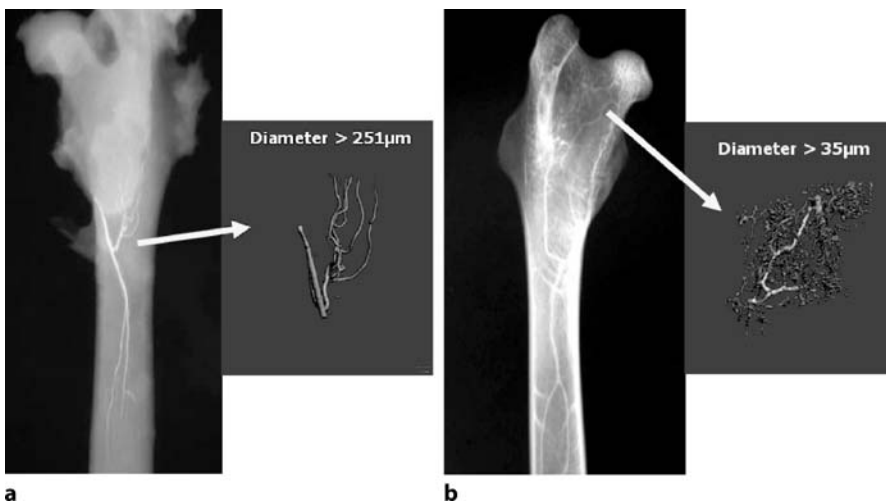


Figure 2a,b. Comparison of two perfusion mediums for in vivo angiography. **a** Perfusion with clinically used barium sulfate only reached vessels in diaphysis larger than 251 µm (arrow) as measured by micro-CT. **b** Perfusion with Microfil lead chromate reached small vessels (arrow) in proximal femur as measured by micro-CT used for this study

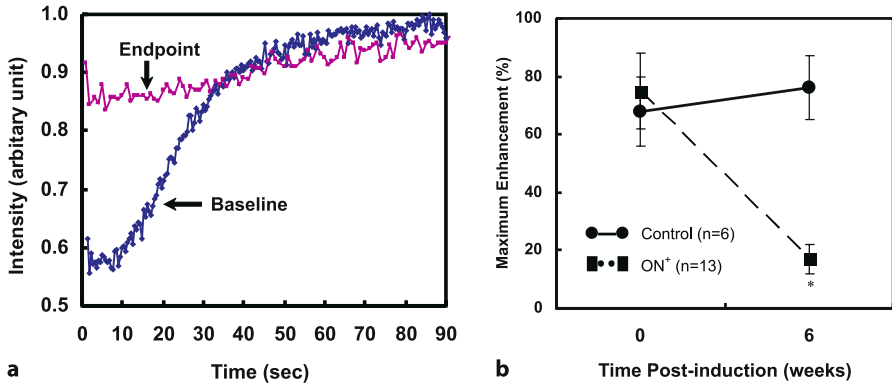


Figure 3. **a** Representative dynamic MRI time-intensity curves of a rabbit with osteonecrotic proximal femur. Significant decrease in the perfusion index “maximum contrast enhancement” found at the end of the experiment as compared with its baseline. **b** Significant decrease in perfusion index maximum contrast enhancement found at proximal femur of the necrotic rabbits as compared with that of the controls. Asterisk: $p < 0.05$, compared with baseline and control rabbits, respectively

dominal aorta distal to the heart with ligation of that proximal to the heart. The vasculature was flushed with 50U/ml heparinized normal saline at 37°C and at a flow speed of 20 mm/min via an automatic pump apparatus (PHD 22/2000, Harvard Apparatus). As soon as the outflow from an incision of the abdominal vein was limp, 10% neutral buffered formalin (37°C) was pumped into the vasculature to fix the nourished skeletal specimen (Bentley et al. 2002; Duvall et al. 2004; Jorgensen et al. 1998; Qin et al. 2006; Simopoulos et al. 2001). The formalin was then flushed from the vasculature using the heparinized normal saline, and the vasculature was injected with clinically used barium sulfate in our pilot study, which was only able to demonstrate diaphysal vessels (Fig. 2a) and was not able to meet our requirement for studying intraosseous vessels at both proximal and distal femura of rabbits; therefore, we adopted the method of others (Bentley et al. 2002; Duvall et al. 2004; Simopoulos et al. 2001) using a lead chromate-containing conformed radiopaque silicone rubber compound based on the manufacturer’s protocol (Microfil MV-122, Flow Tech; Carver, Mass.; <http://www.flowtech-inc.com/microfil.htm>), which demonstrated much better perfusion results for micro-CT scanning of the vessels presented at the metaphysal regions (Fig. 2b).

After completion of perfusion, animals were killed and stored at 4° for 1 h to ensure polymerization of the contrast agent before microangiography. Bilateral femoral samples were then harvested and fixed in paraformaldehyde (4%) for decalcification with Ethylenediaminetetraacetic Acid (EDTA, 10%, pH 7.4). Then, both proximal third and distal third of both femoral samples, i.e., four dissected parts for each rabbit, were obtained for micro-CT scanning and evaluation using μ CT-40 (Scanco Medical, Bassersdorf, Switzerland).

The micro-CT scan was performed perpendicular to the shaft and initiated from a reference line 10 mm away from the bottom with an entire scan length of 10 mm (refer to the X-ray images of Fig. 4a). The scan resolution selected was 36 μm per voxel with 1024 \times 1024 pixel image matrix. For segmentation of blood vessels from background, noise was removed using a low pass Gaussian filter (Sigma = 1.2, Support = 2) and blood vessels was then defined at a threshold of 85. In order to reconstruct 3D architecture of vasculature, the blood vessels filled with Microfil was included with semi-automatically drawn contour at each 2D section. A histogram was subsequently generated to display the distribution of vessel size and a color-coded scale was mapped to the surface of the 3D images to produce a visual representation of the vessel size distribution (Duvall et al. 2004).

Results of Blood Perfusion Imaging Analysis

Pathophysiologic Pathway for Intraosseous Blood Supply

A significant decrease ($p < 0.05$) in the “maximum enhancement” of both proximal and distal femur was found in the ON⁺ rabbits as compared with baseline, whereas no significant change ($p > 0.05$) was found in the control rabbits (Fig. 3).

Micro-CT-Based Evaluation on Intravascular Pathogenic Events

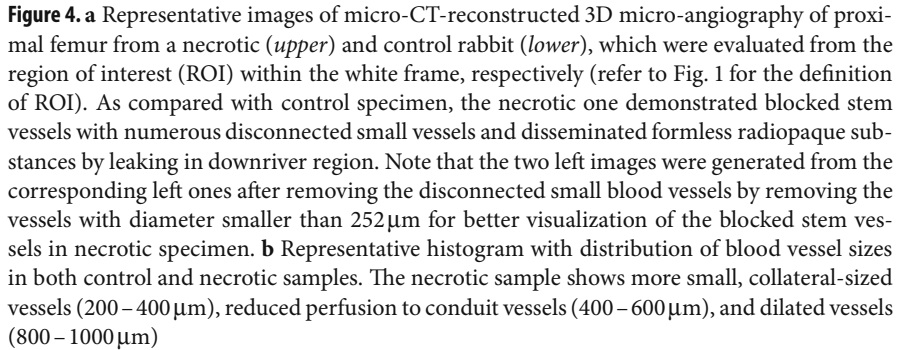
The control samples showed normal vascular network, whereas the ON⁺ samples showed a blocked stem vessel surrounded by small disconnected vessels and disseminated leakage substance (Microfil; Fig. 4a). Quantitatively, histograms were compiled to show the blood vessel size frequency distribution in both ON⁺ samples and the controls. As compared with the control samples, the necrotic ones showed an increase in small, collateral-sized-like vessels (200–400 μm), reduced perfusion to conduit vessels (400–600 μm), and dilated vessels (800–1000 μm ; Fig. 4b).

Discussion and Conclusion

We used advanced bio-imaging methods (dynamic contrast-enhanced MRI and micro-CT-based microangiography) to demonstrate that pathogenic events and pathophysiologic pathways responsible for intraosseous ischemia.

In a pilot study, we also explored if clinical angiography using radiopaque substance barium sulfate would be a better approach to monitor steroid-associated emboli in the intraosseous vascular network; however, due to its larger particle size with lower solubility in solution, only blood vessels larger than 250 μm were visualized to be perfused radiographically. Microfil (lead chromate) is a radiopaque solution with a smaller particle size, which was recently used for quantitative micro-CT analysis of collateral vessel development after ischemic injury (Duvall et al. 2004), and successfully adopted into the present micro-CT angiographic study. Our findings showed that the formation or presence of intravascular thrombosis was well demonstrated by micro-CT-based microangiography, where the thrombi blocked the vasculature

Figure 4. a Representative images of micro-CT-reconstructed 3D micro-angiography of proximal femur from a necrotic (*upper*) and control rabbit (*lower*), which were evaluated from the region of interest (ROI) within the white frame, respectively (refer to Fig. 1 for the definition of ROI). As compared with control specimen, the necrotic one demonstrated blocked stem vessels with numerous disconnected small vessels and disseminated formless radiopaque substances by leaking in downriver region. Note that the two left images were generated from the corresponding left ones after removing the disconnected small blood vessels by removing the vessels with diameter smaller than 252 μm for better visualization of the blocked stem vessels in necrotic specimen. **b** Representative histogram with distribution of blood vessel sizes in both control and necrotic samples. The necrotic sample shows more small, collateral-sized vessels (200–400 μm), reduced perfusion to conduit vessels (400–600 μm), and dilated vessels (800–1000 μm)



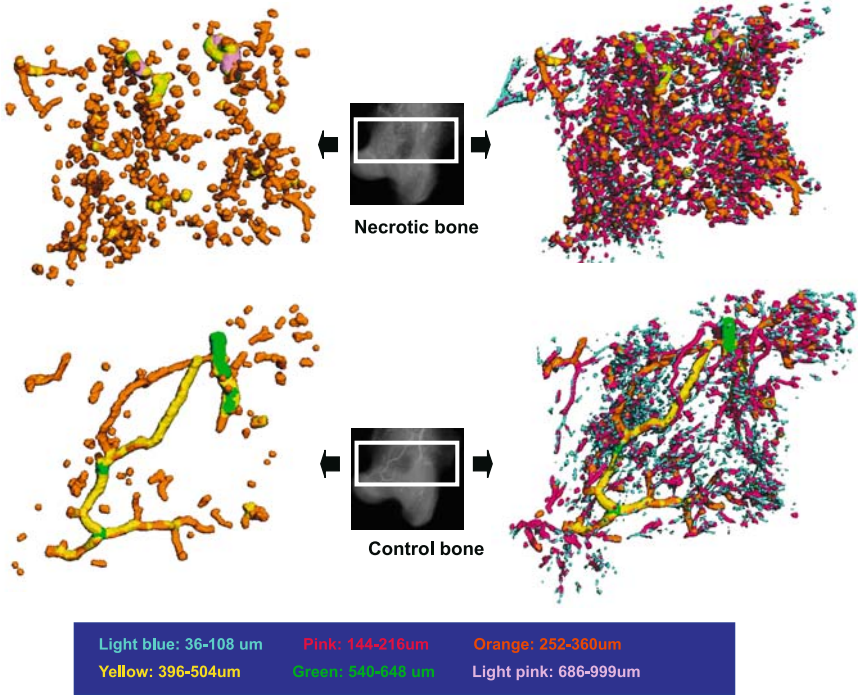
as revealed by both upstream-dilated stem vessels and downstream-reduced conduit vessels localized to the necrotic lesions in decalcified 3D micro-CT intraosseous vascular network.

The above-mentioned perfusion techniques were validated by our previous intravascular hematology and histopathology study, which showed intravascular thrombosis using the same inductive protocol. In ON^+ rabbits, a significant decrease from baseline ($p < 0.05$) induced by LPS was found in the ratio of t-PA/PAI-I before the first MPS injection. Twenty-four hours after the last MPS injection, the decreasing tendency for activated partial thromboplastin time (APTT) was maintained, whereas a rapid decreasing tendency for ratio of t-PA/PAI-I became apparent. It implied imbalance between coagulation and fibrinolysis, such that thrombi occurred histopathologically (Qin et al. 2006).

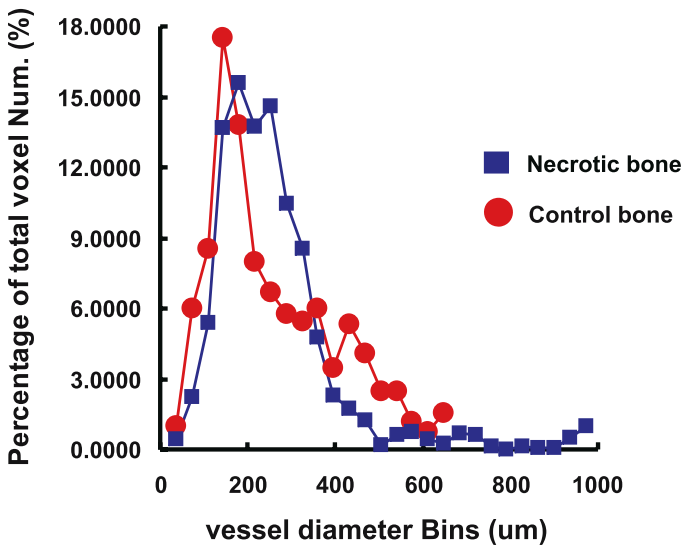
Structural changes of vasculature were also found to be associated with time-course changes in plasma ratio of low-density lipoprotein to high-density lipoprotein (LDL/HDL ratio) in ON^+ rabbits, which showed a significantly increased ratio from the baseline 24 h later after LPS injection, a tendency which was further significantly enhanced 24 h after the last MPS injection. This was evidenced in histopathologic findings, which demonstrated increased fat cell size in the necrotic marrow, accompanied by substantially reduced marrow space (Qin et al. 2006). In fact, higher LDL/HDL ratio was considered to reflect the prominent lipid transport to the peripheral tissues, which might result in extravascular marrow compression from lipid deposition (Glueck et al. 2003).

Both intravascular and extravascular events contributed to the impaired perfusion of intraosseous blood supply. This was evidenced by the significantly decreased “maximum enhancement,” an index of blood perfusion measured by dynamic MRI in ON^+ rabbits in the present study.

The high incidence (93%), and even no mortality, using this protocol might be attributed to both the combined administration of LPS-MPS and a single low-dose LPS. The histopathologic features of ON in this rabbit model were similar to those observed in human ON specimens we obtained from SARS patients (see Fig. 5). The significance of the protocol used in this study with high ON incidence but low or no



a



b

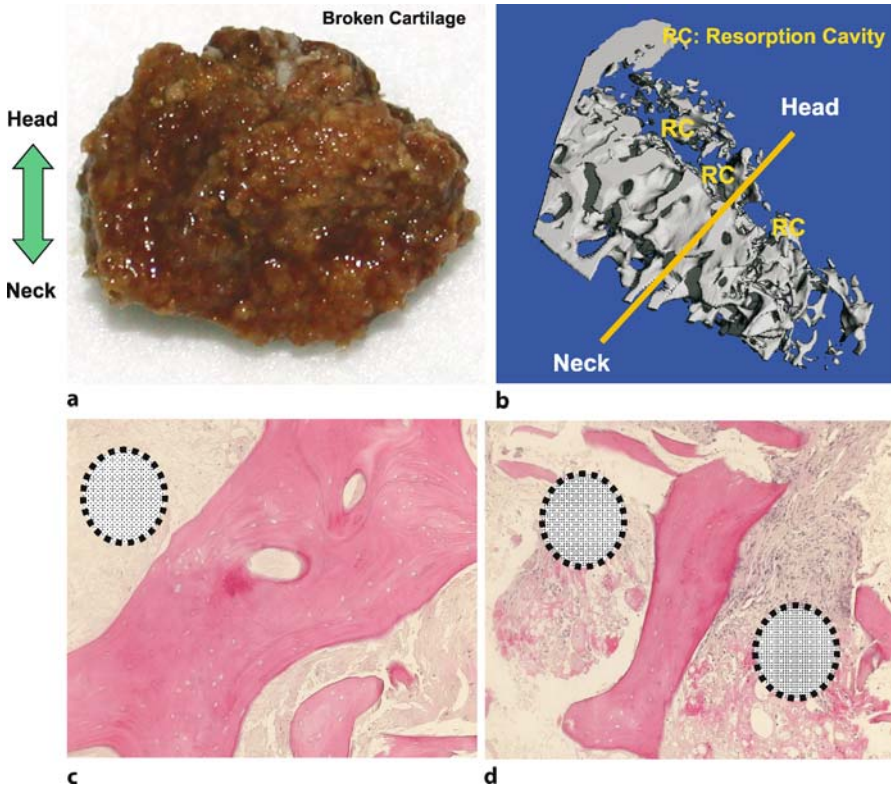


Figure 5 a–d. Osteonecrotic femoral head from a severe acute respiratory syndrome (SARS) patient. **a** Specimen from necrotic femoral head of a patient recovered from SARS. **b** A 3D reconstruction of subchondral necrotic lesion with resorption cavity by micro-CT. **c** Histopathologic section with fibrotic scar formation around the necrotic bone within the *dotted circle* (H&E staining, $\times 200$). **d** Histopathological section with granulation tissue penetration into the necrotic bone with resorption cavity within the *dotted circles* (H&E staining, $\times 200$). RC resorption cavity

mortality was obvious, at least in terms of reducing the number of experimental animals required for intervention at studies and increasing the validity of the evaluation results (Motomura et al. 2004).

In conclusion, static and dynamic bio-imaging modalities, including advanced contrast-enhanced dynamic MRI and micro-CT-based angiography, were unique and non-destructive for studying local blood perfusion. The present experimental study showed that our experimental protocol with a single injection of low-dose LPS and subsequent pulsed high-dose MPS injections were an effective way to induce ON in rabbits with a high incidence and no mortality. The ON model established in the present study therefore forms a solid foundation for investigating the efficacy of potential intervention strategies for prevention of steroid-associated ON.

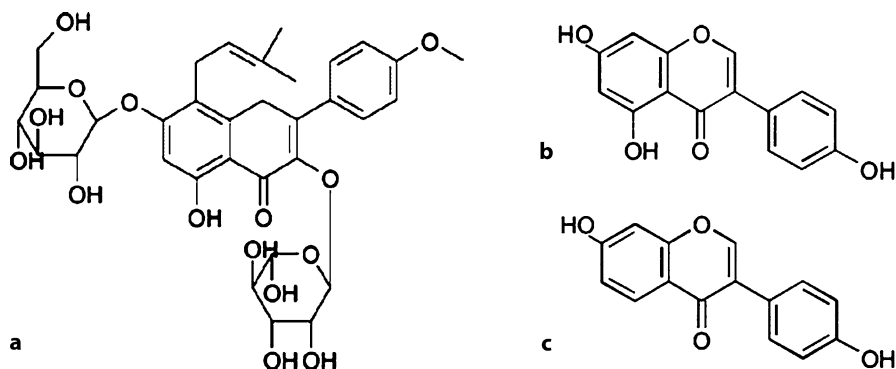


Figure 6a–c. Chemical structures of three main phytoestrogenic components in herbal Epimedium-derived phytoestrogen extraction (HEPE). **a** Icariin (50%). **b** Genistein (2.5%). **c** Daidzein (12.5%)

HEPE Developed for Prevention of Steroid-Associated ON in Rabbit Model

Materials and Methods

Grouping and Treatment

Thirty 28-week-old male New Zealand white rabbits received an established steroid-associated ON inductive protocol as described and also as published recently (Qin et al. 2006). Animals were then divided into control group (CO; $n = 14$) and HEPE group ($n = 16$). Rabbits in HEPE group received HEPE ($5 \text{ mg/kg/bw day}^{-1}$) at the first day of intervention. The known bioactive compounds in HEPE in 5 mg HEPE contained $2500 \mu\text{g}$ Icariin, $125 \mu\text{g}$ Genistein, $625 \mu\text{g}$ Daidzein, and $1750 \mu\text{g}$ vehicle; Fig. 6) was commercially available (Tong Ji Tang Pharmacal Company, Gui Zhou, China; Zhang et al. 2006).

Evaluations on Intravascular and Extravascular Events of Intraosseous Pathogenesis

Local Blood Perfusion In Vivo Contrast-enhanced dynamic MRI was performed on both femora for local intraosseous perfusion before LPS injection and 6 weeks after the last injection of MPS. (Details of the method are mentioned above in section on ON model evaluation.)

Micro-CT-Based Microangiography Six weeks after inductive injection, both femora were dissected after decalcification.

Histopathology After microangiography, all the decalcified samples were embedded in paraffin, then cut into 6-mm-thick sections along the coronal plane for the proximal parts and the axial plane for the distal parts. The ON lesions and intravascular/extravascular pathologic evidence was evaluated. Sections were stained with hematoxylin/eosin (H&E) for evaluation of osteonecrosis and calculation of fat cell

size. Phosphotungstic acid hematoxylin (PTAH) was the staining specifically employed for examination of fibrin thrombus (Prophet et al. 1992).

Regarding evaluation of ON, entire areas of each dissected part of femoral samples, including epiphysis and metaphysis, were examined for the presence of ON, which were judged blindly by two pathologists based on the characteristic histopathologic features with empty lacunae or pyknotic nuclei of osteocytes in the trabeculae, accompanied by surrounding necrotic bone marrow (Yamamoto et al. 1995, 1997). All rabbits that had at least one ON lesion in the examined sections were defined as ON⁺, whereas those with no ON lesions were ON⁻.

Regarding calculation of extravascular marrow fat cell size, the fat cell size of each rabbit was calculated as the average of the Feret's diameter of all bone marrow fat cells with clearly defined profile of each dissected part of the femur samples. The histologic sections were digitized into a microscope imaging system (Zeiss Aixoplan with Spot RT digital camera, Zeiss, Germany) for quantification using image analysis software (ImageJ 1.32j, National Institutes of Health, Bethesda, Md.).

Hematology A 5-ml blood sample was collected in a fasting state from each rabbit through the auricular arteries immediately before injection of LPS, and at weeks 1 and 2 after LPS injection. Half was stored at -70°C for evaluating intravascular thrombotic status, including t-PA/PAI-I (ratio of tissue-type plasminogen activator to plasminogen activator inhibitor) as intravascular fibrinolysis indicator by enzyme-linked immunosorbent assay technique using corresponding mouse monoclonal anti-human antibodies (Manufacturer's Datasheet, Xitang Biotechnology, Shanghai, China) and APTT as intravascular coagulation indicator by Automatic Blood Coagulation Analysis Apparatus (SysmexCA-50, Japan).

Statistics Comparison of the incidence of ON between the control group and the HEPE group was performed using Fisher's exact probability test. Student's *t*-test was used to compare the difference in all the histopathologic measurement data between the control group and the HEPE group. The longitudinal data of dynamic MRI perfusion parameter from each group were analyzed by the program "General Linear Model Based Repeated Measures." All data were expressed as the mean \pm SD and statistical significance was set at $p < 0.05$.

Results

End-Point Evaluations for Safety and Efficacy

Safety No rabbits died in either group throughout the experimental period. Rabbits in the HEPE group were found to be physically more active compared with control rabbits.

Treatment Efficacy The incidence of ON in the HEPE group was 31% (5 of 16), which was significantly lower than 93% (13 of 14) in the CO group ($p < 0.05$). The ON lesions with typical features were found in all the ON⁺ rabbits (Fig. 7).

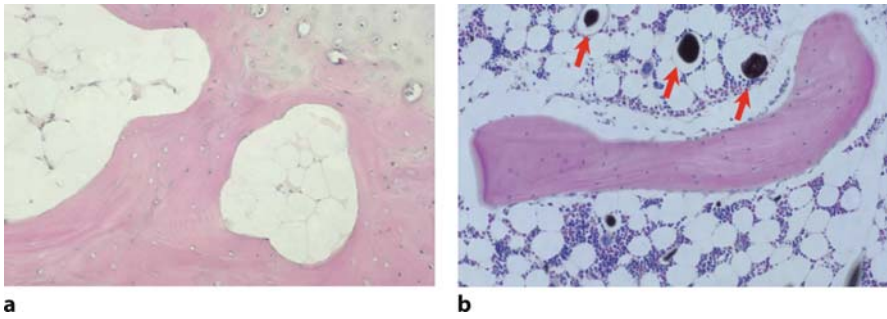


Figure 7 a,b. Histopathologic features compared between representative ON⁺ sample in the non-treatment ON group and representative ON⁺ sample in the HEPE group. **a** Representative ON⁺ sample in the non-treatment control group characterized by more empty lacunae in the trabecular matrix, which were surrounded by more and larger marrow fat cells. **b** Representative ON⁺ sample in the HEPE group showed vital bone with normal osteocytes. Considerable space was preserved for marrow hematopoietic cells and vessels containing radiopaque substance (Microfil), indicated by arrows

Pathophysiologic Pathway for Intraosseous Blood Supply Dynamic MRI-based perfusion study showed that the maximum enhancement at both proximal and distal femur decreased significantly from baseline in the CO group, whereas no change was found at those sites in the HEPE group ($p < 0.05$; Fig. 8).

Regarding the micro-CT-based vascular network, the ON⁺ samples in the CO group showed a blocked stem vessel surrounded by many small disconnected ves-

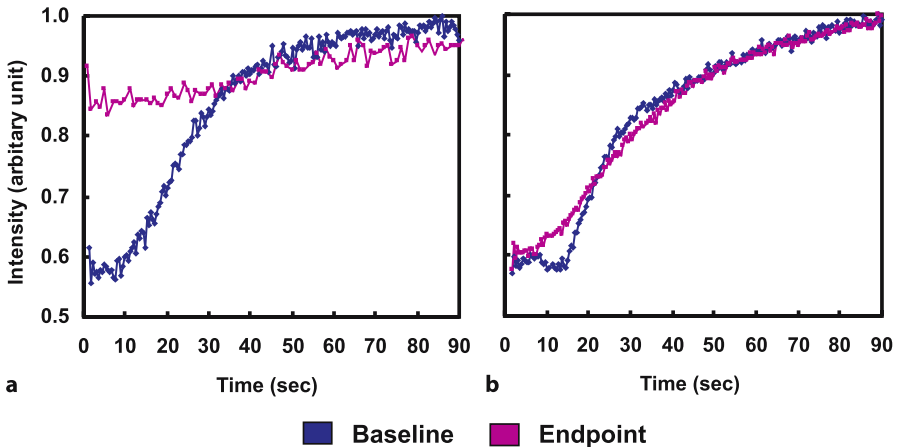


Figure 8 a,b. Representative time-intensity curves (arbitrary unit) by dynamic MRI on proximal femur. **a** Maximum enhancement showed a significant decrease in perfusion function in the non-treatment control group. **b** No significant alteration in perfusion function was found in the HEPE group

sels and disseminated leakage of contrast material (Microfil), whereas there was no blocked stem vessel in the ON⁻ samples of the HEPE group.

Intravascular/Extravascular Pathogenic Events

Intravascular Hematologic Indicators For coagulation, the APTT in the CO group showed a significant decrease from baseline at week 1 after LPS injection and increased towards baseline later, whereas a prominently attenuated tendency was found in the PE group than the CO group throughout the experimental period ($p < 0.05$). For fibrinolysis, the tPA/PAI-I in the CO group significantly declined from baseline at week 1 after LPS injection and increased towards baseline later, whereas an evidently attenuated tendency was found in the PE group throughout the experimental period ($p < 0.05$; Fig. 9).

Extravascular Histopathologic Indicators Histopathologically, the Feret's diameter of marrow fat cell in the HEPE group ($48.17 \pm 3.54 \mu\text{m}$) was significantly smaller ($p < 0.05$) than that in the control group ($63.71 \pm 6.41 \mu\text{m}$). In the HEPE group, considerable space was preserved for marrow hematopoietic cells and vessels in ON⁻ rabbits; however, little space was left for marrow elements due to enlarged fat cell size in the ON⁺ rabbits of the control group (Figs. 7, 10).

Discussion and Conclusion

The present study shows, for the first time, that the herbal Epimedium-derived phytoestrogenic extract (HEPE) was able to prevent steroid-associated ON through

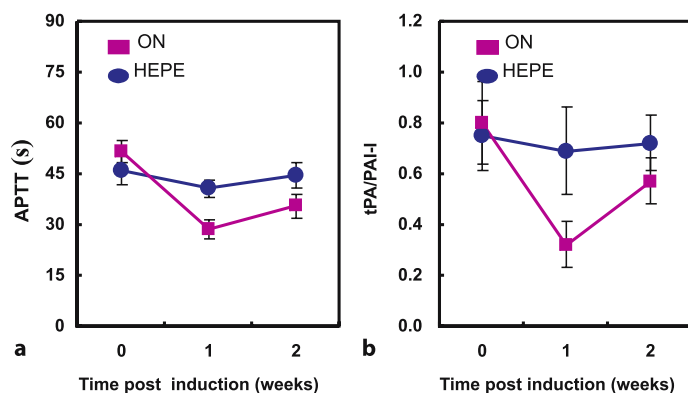


Figure 9a,b. Hematologic data compared between both non-treatment control group and the HEPE group. **a** Significant decrease in APTT found in non-treatment ON group (ON) at week 1 after LPS injection and restored back to the baseline level afterwards, whereas no significant fluctuation was shown in the HEPE group. **b** The tPA/PAI-I in the non-treatment ON group significantly declined from baseline after LPS injection, whereas there were no measurable changes in HEPE treated group. *Asterisk:* significant difference compared between two groups

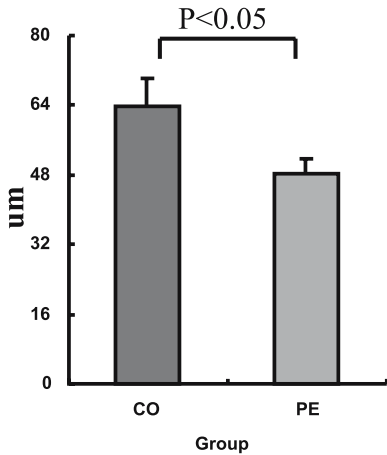


Figure 10. Size of the fat cell was significantly larger in the non-treatment ON group than that of the HEPE group ($p < 0.05$)

a unique mechanism associated with inhibition of both thrombosis and lipid deposition.

In the present study, a single daily oral administration of HEPE effectively reduced threefold the ON incidence (31%) as compared with the control group (93%). Neither animal death nor bleeding event were documented in the HEPE-treated rabbits throughout the experimental period. This may suggest a potential long-term clinical application with more required safety than the available anticoagulants tested clinically (Motomura et al. 2004). Our results may also support, or partially explain, the clinical observations of significantly lower ON incidence in SARS patients in the two cities (Hong Kong and Guang Zhou) in southern China (5–6%; Griffith et al. 2005; Shen et al. 2004) as compared with that in a northern city (Beijing) in China (32.7%; Li ZR et al. 2005), as herb preparations were much more frequently given to SARS patients during pulsed steroid treatment in southern than in northern China (Lau et al. 2005; Liu et al. 2006), apart from steroid dose variations.

The effects of HEPE on the final pathophysiologic pathway to ON, i.e., an impaired structure-function of intraosseous blood supply system, were confirmed by contrast-enhanced dynamic MRI and micro-CT-based angiography. Our findings indicate the potential of HEPE in maintaining local blood circulation and vasculature integrity, functionality, and structure. Functionally, MRI intraosseous perfusion parameter time/intensity-curve-derived maximum enhancement showed a higher value in the examined sites of the ON⁻ rabbits in the HEPE group than those of the ON⁺ rabbits in the control group. Structurally, microangiography showed the capability of HEPE to maintain intraosseous vasculature, as evidenced by no blocked stem vessels in ON⁻ samples of the HEPE group compared with ON⁺ samples in the CO group.

The mechanistic pathway of HEPE was also indicated by its effects on both intravascular and extravascular events. Histopathologically, fat cell size has been commonly defined as a direct indicator of local lipid deposition (Miyanishi K et al. 2001). In the present study, HEPE was shown to be able to inhibit local lipid deposition,

which was evidenced by smaller fat cell size in the HEPE group than the CO group ($p < 0.05$). Hematologically, it suggested that intravascular indicators (both APTT and tPA/PAI-1) implied that HEPE prevented ON development partially via a potential pathway maintaining balance between coagulation and fibrinolysis. Recent experimental findings indicate that pulsed steroids stimulate adipocytic pathway in marrow (Li X et al. 2005), and phytoestrogen showed potential inhibition effects on adipogenesis (Cooke and Naaz 2005; Dang et al. 2003; Dang and Lowik 2004). Our unpublished preliminary *in vitro* data has also demonstrated significantly decreased adipogenic PPAR γ_2 gene expression in marrow cells from steroid-associated ON rabbits with HEPE prevention.

In this study, HEPE decreased ON incidence to 31%, whereas a combination of anticoagulant plus a lipid-lowering agent decreased ON incidence to 5% in an experimental study (Motomura et al. 2004); however, the combination of therapeutics in Motomura's study started 1-2 weeks before inductive injection, and HEPE in our study started immediately before inductive injection. So, direct comparisons between those two experimental studies could not be made. The first limitation of our study was that it was without a dose-effect design, and the prevention efficacy profile of HEPE, thus far, remains unclear.

In conclusion, we provide evidence supporting our hypothesis that HEPE was able to prevent steroid-associated ON in rabbits through a unique mechanism associated with inhibition of both thrombosis and lipid deposition.

Conclusion

We developed a steroid-associated ON rabbit model with high ON incidence and no mortality. This experimental ON model was adopted for efficacy study on an herbal Epimedium-derived phytoestrogenic extract (HEPE) developed for prevention of steroid-associated ON. The underlying mechanisms of HEPE for prevention of steroid-associated ON were found to be inhibition of both intravascular thrombosis and extravascular bone marrow lipid deposition, evaluated using both conventional and advanced bio-imaging techniques, including contrast-enhanced dynamic MRI and a high-resolution micro-CT. Our experimental results support further clinical study and the potential application of HEPE in the prevention of ON development in high-risk patients undergoing steroid treatment.

Acknowledgements This study was supported by a Direct Research Grant of the Chinese University of Hong Kong project ID ref. 6901559) and RGC (CUHK4503/06M).

References

- Aaron RK (1998) Osteonecrosis: etiology, pathophysiology and diagnosis. In: Callaghan JJ, Rosenberg AG, Rubash HE (eds) *The adult hip*. Lippincott-Raven, Philadelphia, p 457
- Anderson JW, Johnstone BM, Cook-Newell ME (1995) Meta-analysis of the effects of soy protein intake on serum lipids. *N Engl J Med* 333:276-282

- Assouline-Dayana Y, Chang C, Greenspan A, Shoenfeld Y, Gershwin ME (2002) Pathogenesis and natural history of osteonecrosis. *Semin Arthritis Rheum* 32:94–124
- Bentley MD, Ortiz MC, Ritman EL, Romero JC (2002) The use of microcomputed tomography to study microvasculature in small rodents. *Am J Physiol Regul Integr Comp Physiol* 282:1267–1279
- Choo MK, Park EK, Yoon HK, Kim DH (2002) Antithrombotic and antiallergic activities of daidzein, a metabolite of puerarin and daidzin produced by human intestinal microflora. *Biol Pharm Bull* 25:1328–1332
- Clifton-Bligh PB, Baber RJ, Fulcher GR, Nery ML, Moreton T (2001) The effect of isoflavones extracted from red clover (Rimostil) on lipid and bone metabolism. *Menopause* 8:259–265
- Cooke PS, Naaz A (2005) Effects of estrogens and the phytoestrogen genistein on adipogenesis and lipogenesis in males and females. *Birth Defects Res A Clin Mol Teratol* 73:472–473
- Dang Z, Lowik CW (2004) The balance between concurrent activation of ERs and PPARs determines daidzein-induced osteogenesis and adipogenesis. *J Bone Miner Res* 19:853–861
- Dang ZC, Audinot V, Papapoulos SE, Boutin JA, Lowik CW (2003) Peroxisome proliferator-activated receptor gamma (PPARgamma) as a molecular target for the soy phytoestrogen genistein. *J Biol Chem* 278:962–967
- Duvall CL, Robert Taylor W, Weiss D, Guldberg RE (2004) Quantitative microcomputed tomography analysis of collateral vessel development after ischemic injury. *Am J Physiol Heart Circ Physiol* 287:302–310
- Expert Panel on Detection, Evaluation, and Treatment of High Blood Cholesterol in Adults (adult treatment panel III) (2001) Executive summary of the third report of the National Cholesterol Education Program (NCEP) *J Am Med Assoc* 285:2486–2497
- Glueck CJ, Freiberg RA, Sieve L, Wang P (2005) Enoxaparin prevents progression of stages I and II osteonecrosis of the hip. *Clin Orthop Relat Res* 435:164–170
- Griffith JF, Antonio GE, Kumta SM, Hui DS, Wong JK, Joynt GM, Wu AK, Cheung AY, Chiu KH, Chan KM, Leung PC, Ahuja AT (2005) Osteonecrosis of hip and knee in patients with severe acute respiratory syndrome treated with steroids. *Radiology* 235:168–175
- Hong N, Du XK (2004) Avascular necrosis of bone in severe acute respiratory syndrome. *Clin Radiol* 59:602–608
- Irisa T, Yamamoto T, Miyanishi K, Yamashita A, Iwamoto Y, Sugioka Y, Sueishi K (2001) Osteonecrosis induced by a single administration of low-dose lipopolysaccharide in rabbits. *Bone* 28:641–649
- Jorgensen SM, Demirkaya O, Ritman EL (1998) Three-dimensional imaging of vasculature and parenchyma in intact rodent organs with X-ray micro-CT. *Am J Physiol Heart Circ Physiol* 275:1103–1114
- Koller E, Mann M, Malozowski S, Bacsanyi J, Gibert C (2000) Aseptic necrosis in HIV seropositive patients: a possible etiologic role for megestrol acetate. *AIDS Patient Care STDS* 14:405–410
- Lamon-Fava S (2000) Genistein activates apolipoprotein A-I gene expression in the human hepatoma cell line Hep G2. *J Nutr* 130:2489–2492
- Lang P, Jergesen JE, Genant HK, Moseley ME, Schuyte-Monting J (1989) Magnetic resonance imaging of the ischemic femoral head in pigs. Dependency of signal intensities and relaxation times on elapsed time. *Clin Orthop Relat Res* 244:272–280
- Lau TF, Leung PC (2005) Using herbal medicine as a means of prevention experience during the SARS crisis. *Am J Chinese Med* 33:345–356
- Lee SH, Jung BH, Kim SY, Chung BC (2004) Determination of phytoestrogens in traditional medicinal herbs using gas chromatography-mass spectrometry. *J Nutr Biochem* 15:452–460

- Li X, Jin L, Cui Q, Wang GJ, Balian G (2005) Steroid effects on osteogenesis through mesenchymal cell gene expression. *Osteoporos Int* 16:101–108
- Li ZR, Sun W, Qu H, Zhou YX, Dou BX, Shi ZC, Zhang NF, Cheng XG, Wang DL, Guo WS (2005) Clinical research of correlation between osteonecrosis and steroid. *Zhonghua Wai Ke Za Zhi* 43:1048–1053
- Lieberman JR, Berry DJ, Montv MA, Aaron RK, Callaghan JJ, Rayadhyaksha A, Urbaniak JR (2002) Osteonecrosis of the hip: management in the twenty-first century. *J Bone Joint Surg Am* 84:834–853
- Liu X, Zhang M, He L, Li YP, Kang YK (2006) Chinese herbs combined with Western medicine for severe acute respiratory syndrome (SARS). *Cochrane Database Syst Rev*:CD004882
- Martin JL, Fry ET, Sanderink GJ, Atherley TH, Guimart CM, Chevalier PJ, Ozoux ML, Pensyl CE, Bigonzi F (2004) Reliable anticoagulation with enoxaparin in patients undergoing percutaneous coronary intervention: the pharmacokinetics of enoxaparin in PCI (PEPCI) study. *Catheter Cardiovasc Interv* 61:163–170
- Meng FH, Li YB, Xiong ZL, Jiang ZM, Li FM (2005) Osteoblastic proliferative activity of *Epimedium brevicornum Maxim.* *Phytomedicine* 12:189–193
- Miller KD (2002) High prevalence of osteonecrosis of the femoral head in HIV infected adults. *Ann Intern Med* 137:17–25
- Motomura G, Yamamoto T, Miyanishi K, Jingushi S, Iwamoto Y (2004) Combined effects of an anticoagulant and a lipid-lowering agent on the prevention of steroid-induced osteonecrosis in rabbits. *Arthritis Rheum* 50:3387–3391
- National Osteonecrosis Foundation website. <http://www.nonf.org/index.html>
- Pritchett JW (2001) Statin therapy decreases the risk of osteonecrosis in patients receiving steroids. *Clin Orthop Relat Res* 386:173–178
- Prophet EB, Mills B, Arrington JB, Sobin LH (eds) (1992) *Armed Forces Institute of Pathology Laboratory Methods in Histotechnology*. American Registry of pathology, Washington DC, p 98
- Qin L, Zhang G, Shi YY, Lee KM, Leung PC (2005a) Prevention and treatment of osteoporosis with traditional herbal medicine. In: Deng HW et al. (eds) *Current topics of osteoporosis*. World Scientific, UK, pp 513–531
- Qin L, Zhang G, Hung WY (2005b) Phytoestrogen-rich Herb Formula “XLGB” prevents OVX-induced deterioration of musculoskeletal tissues at hip in old rats. *J Bone Miner Metabol* 23S:55–61
- Qin L, Zhang G, Sheng H (2006) Multiple imaging modalities in evaluation of experimental osteonecrosis induced by a combination of lippolysaccharide and methylprednisolone. *Bone* 39:863–871
- Saito S, Saito M, Nishina T, Ohzono K, Ono K (1989) Long-term results of total hip arthroplasty for osteonecrosis of the femoral head. A comparison with osteoarthritis. *Clin Orthop Relat Res* 244:198–207
- Schulman S (1999) The effect of the duration of anticoagulation and other risk factors on the recurrence of venous thromboembolisms. Duration of Anticoagulation Study Group. *Wien Med Wochenschr* 149:66–69
- Scribner AN, Troia-Cancio PV, Cox BA, Marcantonio D, Hamid F, Keiser P, Levi M, Allen B, Murphy K, Jones RE, Skiest DJ (2000) Osteonecrosis in HIV: a case-control study. *J Acquir Immune Defic Syndr* 25:19–25
- Shen J, Liang BL, Zeng QS, Chen JY, Liu QY, Chen RC, Zhong NS (2004) Report on the investigation of lower extremity osteonecrosis with magnetic resonance imaging in recovered severe acute respiratory syndrome in Guangzhou. *Zhonghua Yi Xue Za Zhi* 84:1814–1817

- Simopoulos DN, Gibbons SJ, Malysz J, Szurszewski JH, Farrugia G, Ritman EL, Moreland RB, Nehra A (2001) Corporeal structural and vascular micro-architecture with X-ray micro-computerized tomography in normal and diabetic rabbits: histopathological correlation. *J Urol* 165:1776–1782
- So LK, Lau AC, Yam LY, Cheung TM, Poon E, Yung RW, Yuen KY (2003) Development of a standard treatment protocol for severe acute respiratory syndrome. *Lancet* 361:1615–1617
- Wang GJ (2000) The pathogenesis and prevention of steroid-induced osteonecrosis. *Clin Orthop* 370:295–310
- Wang W, Zhu GJ, Zu SY (2004) Effects of 17β Estradiol and Phytoestrogen α -Zearalanolone on coagulation and fibrinolysis in Rats. *Chin J Arterioscler* 12:139–142
- Wortmann RL (2002) Lipid-lowering agents and myopathy. *Curr Opin Rheumatol* 14:643–647
- Yamamoto T (1997) Effects of pulse methylprednisolone on bone and marrow tissues: corticosteroid-induced osteonecrosis in rabbits. *Arthritis Rheum* 40:2055–2064
- Yamamoto T, Hirano K, Tsutsui H, Sugioka Y, Sueishi K (1995) Corticosteroid enhances the experimental induction of osteonecrosis in rabbits with Shwartzman reaction. *Clin Orthop Relat Res* 316:235–243
- Zhang G, Qin L, Hung WY (2006) Flavonoids derived from herbal *Epimedium Brevicornum* Maxim prevents OVX-induced osteoporosis in rats independent of its enhancement in intestinal calcium absorption. *Bone* 38:818–825